Nowcasting Convective Storm Initiation Using Satellite Based Box-Averaged Cloud Top Cooling and Cloud Type Trends

Justin M. Sieglaff, Lee M. Cronce, Wayne F. Feltz
Cooperative Institute for Meteorological Satellite Studies, University of Wisconsin-Madison, Madison Wisconsin

Kristopher M. Bedka
Science Systems and Applications, Inc. Hampton, Virginia

Michael J. Pavolonis and Andrew K. Heidinger
NOAA/NESDIS, Satellite Applications and Research (STAR), Advanced Satellite Products Team, Madison, Wisconsin

Corresponding author address: Justin Sieglaff, 1225 West Dayton Street, Madison, Wisconsin 53706. E-mail: justins@ssec.wisc.edu Telephone: 608.265.5357 Fax: 608.262.5974

Submitted to Journal of Applied Meteorology and Climatology
Revisions Submitted, September 7, 2010

ABSTRACT

Short-term (0-1 hour) convective storm nowcasting remains a problem for operational weather forecasting and convective storms pose a significant monetary sink for the aviation industry. Numerical weather prediction models, traditional meteorological observations, and radar are all useful for short-term convective forecasting, but all have shortcomings. Geostationary imagers, while having their own shortcomings, are valuable assets for addressing the convective initiation nowcast problem. The University of Wisconsin Convective Initiation (UWCI) nowcasting algorithm is introduced for use as an objective, satellite-based decision support tool. The UWCI algorithm computes GOES Imager infrared window channel box-averaged cloud top cooling rates and creates convective initiation nowcasts based on a combination of cloud top cooling rates and satellite-derived cloud top type/phase trends. The UWCI approach offers advantages over existing techniques, such as increased computational efficiency (decreased runtime) and day/night independence.

A validation of the UWCI algorithm relative to cloud-to-ground lightning initiation events is also presented for 23 convective afternoons and 11 convective nights over the central United States during April, May, June, and one night of July during 2008 and 2009. The mean probability of detection and false alarm ratio are 56.3% (47.0%) and 25.5% (34.8%), respectively, for regions within a Storm Prediction Center severe storm risk area (entire validation domain). The UWCI algorithm is shown to perform: 1) better in regimes with storms developing in previously clear to partly cloudy skies and along sharp boundaries, and 2) poorer in other regimes such as scenes covered with cirrus shields, existing convective anvils, and fast cloud motion.

1. Introduction

Predicting the timing and location of the initial development of thunderstorms (i.e. convective initiation) is a difficult problem of operational forecasters. For deep convection to occur, there must be sufficient moisture in the lower troposphere, steep lapse rates, and there must be sufficient lift of parcels from the low moist layer to the parcel's level of free convection (Johns and Doswell 1992). The challenge of the forecaster is to deduce the structure between observations in space and time, utilizing the limited sounding data, and to project temporal changes in this structure for the forecast period in question (Moeller 2001). The use of numerical weather prediction models for the prediction of convective development is often problematic, as the specific details of the initiation process are still not well enough understood to represent it within these models (Browning et al. 2007). In addition to numerical output, forecasters can monitor surface convergence boundaries using radar, however this alone does not provide specific information on the timing and location of convection (Roberts and Rutledge 2003). Geostationary satellites, with frequent refresh rates (5-15 minutes) are very useful in monitoring where and when convective initiation will occur. Convective initiation (CI) can be identified through rapid cloud top cooling in geostationary satellite infrared imagery 30-45 min in advance of significant precipitation echoes detected by ground-based radar (Roberts and Rutledge 2003). In addition, an understanding of the thermodynamic environment in locations where signals of CI are observed could help to provide significant lead time in the forecasting of thunderstorm hazards such as flash flooding, high winds, large hail, and tornadoes (Koenig and de Coning 2008; Wagner et al. 2008).

In addition to the operational forecasting challenges, thunderstorms account for most of the air traffic delays in the United States and cost the aviation industry many millions of dollars annually in lost time, fuel, and efficiency through delayed, canceled, and rerouted flights (Kaplan et al. 1999; Murray 2002; Mecikalski et al. 2007). Therefore, knowledge of when and where CI is occurring based upon satellite observations can benefit the aviation industry through improvements in safety and efficiency.

Objective methods for nowcasting CI using geostationary satellite imagery have recently been developed. One CI nowcasting approach described by Mecikalski and Bedka (2006, MB06 hereafter) involves the combination of mesoscale atmospheric motion vectors (AMVs, Bedka and Mecikalski 2005) and a daytime-only convective cloud mask (Berendes et al. 2008) to identify newly developing convective storms in sequential Geostationary Operational Environmental Satellite (GOES) Imager observations (Menzel and Purdom 1994). They utilize a set of multispectral CI nowcast criteria (or "interest fields") including ~11 μm infrared window channel (IR-window) brightness temperature (BT) values/trends coupled with band difference values/trends that are used as a proxy for cloud top height and upper tropospheric moisture content. Sub-freezing IR-window BT values are used as a proxy for cloud top glaciation, which are shown by Roberts and Rutledge (2003) to correlate well with the onset of precipitation from a rapidly developing convective cloud. While this approach has shown some skill for CI nowcasting (Mecikalski et al. 2008), it is not well suited for real-time stand-alone operational decision support because it is limited to daytime only scenes

and produces significant false alarm (~70%), making differentiation between useful CI nowcast signal and algorithm noise/error very difficult.

Other approaches involve the identification and tracking of coherent convective cloud objects to nowcast future evolution. Zinner et al. (2008) describes a daytime-only approach using a combination of visible and IR-window information for CI nowcasting over a central European regional domain. Algorithms such as the "Rapidly Developing Thunderstorms" (RDT, Morel et al. 2002), MASCOTTE (Corvalho and Jones 2001), and ForTraCC (Vila et al. 2008) are primarily designed to nowcast intensification, areal coverage, and movement of convective clouds that are at a more mature stage of development than those that are the focus of MB06 and Zinner et al.

There is a clear need to expand CI nowcasting capability to both the day and night, as hazardous storms such as mesoscale convective systems (MCS, Maddox 1980) often initiate and evolve during the night-time hours. This paper describes a new day/night CI nowcasting approach developed at the University of Wisconsin Cooperative Institute for Meteorological Satellite Studies (UW-CIMSS) using the concept of "box-averaging" to compute IR-window channel cloud top cooling rate and cloud top type trends derived from multispectral GOES data. The cloud top type information used within the UW-CIMSS CI (UWCI) nowcast algorithm was developed by the GOES-R Advanced Baseline Imager (ABI) Cloud Algorithm Working Group (AWG) for future operational use with ABI data at NOAA/NESDIS, as well as an analogous algorithm to operate on more spectrally limited current GOES Imagers. The UWCI algorithm has an advantage over other CI nowcast methods in that it can operate very efficiently over an

entire full disk during both day and night utilizing high temporal resolution (5 to 15-minute) and state-of-the-art cloud type retrievals.

The UWCI nowcast algorithm is demonstrated and validated against cloud-to-ground (CG) lightning strike data during portions of the spring and early summer of the 2008 and 2009 over the central U.S. The CG validation aims to assess the accuracy of the UWCI algorithm for nowcasting the first occurrence of CG lightning (i.e. lightning initiation) and to understand the characteristics of new lightning producing storms in IR-window satellite imagery. CG lightning data serves a proxy for convective initiation in this study instead of radar reflectivity. Previous studies have shown storm electrification occurs on average, 7.2 minutes after a storm achieves 40 dBZ radar reflectivity (Dye et al. 1989). Given this lag between storm electrification and 40 dBZ radar echoes, the lead-times shown within this paper are slightly inflated compared to a 35-40 dBZ radar echo threshold. Cloud-to-ground lightning offers a binary yes/no validation source with continuous coverage over the entire validation domain. Radar coverage is extensive over the United States, but there are scan gaps due to radar placement, beam blockage, and beam curvature away from radar locations. Additionally, a radar dBZ threshold for convective initiation definition is arbitrary. A lightning strike signifies a significant convective updraft, however the same is not necessarily true in presence of a 35+ dBZ radar echo. Object tracking techniques using the Warning Decision Support System – Integrated Information (WDSS-II, Lakshmanan, et al. 2007) are being developed, which will allow radar, cloud-to-ground lightning, and satellite to be coupled together for direct automated validation, but such methods are not sufficiently developed for use in this study.

The following sections describe: 1) the satellite and lightning datasets used in this study, 2) the UWCI algorithm methodology, 3) validation and discussion of the UWCI nowcasts with respect to CG lightning initiation, and 4) conclusions from this study.

2. Datasets

a. GOES-12 Imager Data

Multispectral GOES-12 Imager satellite data is the primary dataset used within this study. These data are used by the cloud type algorithm (described below) and UWCI algorithm. This study uses GOES-12 data over the U.S. Central and Southern Plains from the 1815 to 2345 UTC time period for 23 convective afternoons and 0015 to 0615 UTC for 11 convective nights during April, May, June, and one night in July of 2008 and 2009 (see Tables 1 and 2 for lists of these days). The domain of interest covers a region from 30°N to 46°N and 94°W to 104°W. CI occurred during the time periods of interest for the validation days and many of the clouds evolved into mature thunderstorms with surface severe weather reports, including large hail (0.75 inch diameter or larger), damaging winds (50 knots or greater), and/or tornadoes.

b. Cloud Type Product

The cloud type algorithm classifies each GOES pixel into one of the following categories: clear, liquid water, supercooled liquid water, mixed phase, opaque ice, non-opaque ice, and multilayered ice cloud (ice cloud is the highest cloud layer). These categories are described in detail in Pavolonis and Heidinger (2004) and Pavolonis et al. (2005). The daytime only approach in Pavolonis and Heidinger (2004) and Pavolonis et

al. (2005) is improved to an IR-only, day/night independent approach with the theory described within Pavolonis (2010a) and algorithm details described in Pavolonis (2010b). The approach utilizes clear-sky background correction (including surface emissivity and atmospheric gaseous absorption), accounts for satellite zenith angle, and incorporates sensor spectral response functions. These attributes allow for the cloud mask and type algorithm to be portable to many sensors with similar channels and regardless of satellite zenith angle. Most relevant to this study is the identification of glaciated cumulus clouds, which fall into the opaque ice, non-opaque ice, or multilayered ice cloud categories. The cloud type algorithm relies on an upfront cloud mask algorithm to determine which pixels contain cloud. The cloud mask is described in Heidinger (2010). An example of the cloud type product is shown in Figure 1. The false color image allows inference of cloud type, purple/pink clouds are ice, white/yellow clouds are water and green is land. Only infrared radiances are used, so the cloud type algorithm is independent of solar zenith angle.

c. NLDN CG Lightning Initiation Dataset

National Lightning Detection Network (NLDN) CG lightning data is used to the determine accuracy of the UWCI algorithm output. Specifically, locations of "lightning initiation" (LI) are derived from the NLDN CG lightning data. The NLDN has been shown to have a flash detection efficiency of 90% with a location accuracy of 500 m (Cummins et al. 1998). Lightning strike locations are shifted to account for the satellite parallax effect, which causes satellite observations of high clouds to be misplaced relative to their actual location above the earth surface (Johnson et al. 1994). A constant cloud

height of 7 km is assumed, resulting in a net shift of all lightning strike locations to better match the locations of the parent cloud and UWCI nowcast pixels.

In this study, LI is defined as the time/location (latitude/longitude) of the first NLDN-observed lightning strike within a newly developing convective cloud. One may argue that a total lightning dataset that includes intra-cloud lightning would be a better validation tool as intra-cloud lightning often precedes CG lightning in developing convective clouds (Goodman et al. 1988). The authors agree, however such a dataset is not yet available over large geographical areas such as the entire Central and Southern Plains of the United States. Experimental Lightning Mapping Array (LMA) networks (Rison et al., 1999) do exist over portions of northern Alabama, central Oklahoma, Florida, Washington DC, and the Dallas/Fort Worth Metropolitan areas (Goodman et al. 2005; Demetriades, et al. 2004), but full CONUS coverage of total lightning will not exist until the launch of the GOES-R satellite with its Geostationary Lightning Mapper instrument (Goodman et al. 2010).

The LI event database was generated manually over the study domain. The CG strike data was grouped into 5-minute intervals and color-coded 60-minute lightning imagery was produced. This lightning strike imagery was used to determine LI locations and times. Newly developing storms are only considered, such as those developing from small cumulus surrounded by clear sky, beneath debris clouds, beneath existing anvils, or new storms developing to the rear of existing storms (i.e. “back-building”). Time sequences of GOES-12 IR-window imagery are used to further verify that the LI has occurred within a newly developing cloud. Storms not included in the LI datasets include storm splits and stray lightning strikes associated with existing thunderstorm anvils.

Figure 2 provides an example of a 5-minute lightning data plot used to identify LI events, valid for 29 April 2009 at 2040 UTC. All lightning strikes between 2037:30 UTC and 2042:29 UTC are plotted in red and the image is given a timestamp of 2040 UTC. Additional 5-minute binned lightning strikes for the past 60 min are also included in lightning plots with different colors. In this example, LI is determined to occur over the west central Texas panhandle at 2040 UTC. This procedure was performed on all days/time periods of interest, yielding 487 total LI events within the validation domain and study time period.

3. UWCI Algorithm Description

a) Background and Motivation

The UWCI algorithm is designed to nowcast newly developing convection in areas not obscured by ice cloud layers/anvils and mid-level cloud layers. Nowcasts from the UWCI algorithm are intended to serve primarily as a decision support tool for operational forecasters, although additional uses may include assimilation into regional numerical weather prediction (NWP) models or other fuzzy logic-based "expert" weather systems (Iskenderian et al. 2009). The algorithm is designed to capture the period from the first signal of cloud vertical growth through the time where the cloud top glaciates and the storm is considered mature. After a developing convective cloud has sufficiently glaciated, the algorithm is designed to 'shut-off' being that it is not designed to nowcast future intensification/decay of mature storms or storm complexes. The ability to nowcast the characteristics of mature convection (e.g. future location, anvil expansion, expected lifetime, intensification/decay) requires an entirely different algorithm framework such as

the object tracking methods described by Carvalho and Jones (2001), Machado and Laurent (2004), Rabin and Whittaker (2006), Morel et al. (2002), and Vila et al. (2008).

The foundation of the UWCI algorithm rests on an approach called "box-averaging". The term "box-average" refers to the computation and time differencing of the mean IR-window BT and cloud type properties within a small box centered on the pixel of interest. The box-average approach is best suited for geostationary imagery due to the frequent refresh rate where cloud motion between consecutive scans is small. Current GOES operational CONUS scans range anywhere from 5 minutes in "rapid scan" mode to 13-17 minutes in "normal operations" (30-minute gaps do occur every 3 hours with current GOES CONUS scans and this addressed later in the text). The future GOES Imager (Advanced Baseline Imager, ABI) will have CONUS scans every 5 minutes (Schmit et al, 2005). For example, the average movement of developing convective clouds over CONUS in "rapid-scan" GOES-12 imagery was 5 km/5 min, with a standard deviation of 2 km/5 min, based upon manual tracking of 50 developing convective clouds across multiple cases (analysis not shown in this paper). Thus, if one places a box of 7x7 4 km GOES-12 pixels (i.e. ~28 x 28 km area at nadir) around a given convective cloud, the cloud could move anywhere within the box at movement speeds near three standard deviations above the mean and still remain in the box. This box size is chosen to compromise between "rapid scan" and "normal operations" of current GOES. These box sizes can result in increased error (e.g.- reduced probability of detection and increased false alarm ratio) for scenes with fast cloud motion and for thirty minute scan gaps associated with current GOES "normal operations" scan pattern. The difference of the box-averaged IR-window BT field between the current and previous scans is used to

reveal areas of cloud top cooling correlated with vertical cloud growth. The box-average methodology does not require the calculation of computationally expensive and sometimes errant AMVs (Bedka et al. 2009), such as those needed in the MB06 methodology, thereby improving algorithm performance and reducing false alarm. The box-averaged method is not perfect and complex logic is required to eliminate false cooling induced by horizontal cloud advection, thin cirrus motion, and complex multi-layer cloud scenes. A detailed description of the algorithm and this filtering process is described in the following section.

b) Algorithm Detail

The UWCI algorithm employs a two-box approach. Centered on each pixel within a GOES Imager scan, a small box (7 x 7 pixels) and a large box (13 x 13 pixels) are considered. The box-averaged IR-window BT is computed for each pixel using the small box. The box-averaged IR-window BT calculation is made using pixels of the following cloud types: water, supercooled water, mixed phase, cirrus, overlap, and thick ice. Clear pixels are omitted because their inclusion would result in a box-average temperature that is not solely an average of the cloudy pixels. An average of only the cloudy pixels is desired since the change in temperature between two scans can be used as a proxy for vertical cloud growth. Inclusion of clear-sky pixels would act to decrease the difference between two scans due to little change in ground temperatures and possible large clear pixel counts within the box. Fog pixels are omitted since these are not typically associated with developing vertical convection. Figure 3 shows an example of

the box-averaged IR-window BT field compared to the IR-window field at native resolution.

A small box is required to be at least 5% cloudy to have a valid box-averaged IR-window BT; otherwise the value is set to missing (black areas in left panel of Fig. 3). The 5% requirement is designed to ensure that more than one IR pixel is contributing to the box-averaged IR-window BT. In addition to the box-averaged IR-window BT, the percentage of each cloud type category is computed for all pixels within the small and large boxes. The percentages of cloud types are later used for clearing false cloud top cooling areas and in assigning a CI nowcast category.

Once the box-averaged IR-window BT fields are computed for the current and previous scan times, the two fields are differenced (current minus previous). This difference is known as the unfiltered cloud top cooling (CTC) rate (Fig. 4). The unfiltered CTC is only computed for pixels with valid box-average IR-window temperature at both the current and previous scan, otherwise it is not possible to calculate a cooling rate. The unfiltered CTC is normalized to a 15-minute CTC rate to account for temporally inconsistent GOES scan patterns. The unfiltered CTC reflects two atmospheric phenomena, horizontal cloud motion and vertical cloud growth. In cases with horizontal cloud advection, a box once occupied by low, warm clouds in the previous scan can contain high, cold clouds at the current scan. When these two are differenced, areas of false cooling are found. Vertically growing clouds that have not moved out of their boxed region would also show up as cooling when time differenced. Isolation of only this vertical growth signal is desired for the final CTC product, so therefore it is

necessary to devise a technique to separate areas of false cooling from areas of true cooling.

The false cooling areas are removed from the unfiltered CTC field to produce a filtered CTC field. This filtering is accomplished by a series of seven tests. If a pixel fails any one of these tests, the cloud-top cooling rate is discarded. The first two tests eliminate the majority of false cloud-top cooling rates. An overview of the flow of these tests and overall algorithm logic is shown in Figure 5.

The first test eliminates areas of false cooling due to cloud motion. This test compares the box-averaged IR-window BT of a given pixel *at the current satellite scan time* to the minimum box-average IR-window BT along periphery of the large box *at the previous satellite scan time*. Periphery (here and in subsequent test descriptions) refers to a single row of box-average IR-window BTs along the perimeter of a box. The box-averaged IR-window BT of the pixel of interest must be less than the minimum box-averaged IR-window BT along the periphery of the large box. If the value is greater than the minimum box-averaged IR-window BT along the periphery of the large box, the CTC value is discarded as the cooling is assumed to be a result of horizontal cloud motion, not vertical cloud growth.

The second test is similar to the first test, except it compares values at the current satellite scan instead of current versus previous satellite scans. The box-averaged IR-window BT for the pixel of interest is compared to and must be less than the minimum box-averaged IR-window BT along the periphery of the large and small boxes. Also, the minimum box-averaged IR-window BT along the periphery of the small box must be smaller than the minimum box-averaged IR-window BT along the periphery of the large

box. Additionally, the pixel-level BT (not box-averaged values) at the pixel of interest must be cooler than the minimum BT along the periphery of the small and large boxes. This test ensures true cooling occurring within developing storm updrafts are retained and false cooling from horizontal cloud advection/expansion is mitigated.

The third test limits areas of CTC to areas where the large box ice cloud percentage at the current scan time is less than 50%, where ice cloud is defined as pixels with thick ice, cirrus, or overlap cloud types. Cooling pixels with ice cloud percentages of 50% or more are eliminated to omit continued cooling of thunderstorm anvils/cirrus canopies.

The fourth test determines areas of potentially false cooling associated with horizontal motion of thin cirrus clouds over generally clear areas or small cumulus fields. In some cases, the edges of thin cirrus clouds can occasionally be classified as water cloud and in other cases there can be small cumulus clouds nearby cirrus clouds. Areas within the large box where only cirrus, overlap, and water clouds are present and where cirrus/overlap clouds exceed the number of water cloud pixels are eliminated. This does not have an adverse impact on maintaining CTC signal for developing convective clouds since water cloud pixels typically far exceed cirrus pixels and other cloud types (supercooled water, mixed phase, and/or thick ice pixels).

The fifth test identifies and removes pixels where unexpected microphysical transitions occur. For new convective storm development, a cloud will progress from water cloud to supercooled/mixed phase cloud and finally to glaciated ice cloud. When boxes contain clouds that do not follow this progression, it is assumed that a new cloud has moved into the box, which can induce error within the CTC field. In areas absent of

thick ice pixels, CTC is omitted when a cloud top is first dominated (greater count of pixels within the box of a certain cloud type over other types) by ice (cirrus/overlap types) and later appears to transition to a cloud with a majority of water/supercooled/mixed phase pixels.

The sixth test identifies and filters areas where overlap cloud type is the dominant cloud type within the small box. The overlap dominated areas are omitted since a lower cloud layer and a semi-transparent (in the IR) higher ice cloud layer both contribute to the BT for an overlap pixel. Therefore, any CTC derived from these pixels cannot necessarily be treated as vertical cloud growth, as the upper layer ice cloud could have simply become thicker between images, producing a colder IR-window BT.

The seventh test determines whether the remaining CTC pixels are considered marginally cooling by a series of four subtests. These pixels are a combination of immature vertically growing clouds and horizontally moving clouds. This seventh test weights the following four subtests, awarding a 'weight number' (indicated in parentheses). If a pixel passes a subtest, a 'weight number' of zero is given for that subtest. The subtests include, the minimum pixel level (not box-averaged values) IR-window BT cooling rate within the entire small box (2), the standard deviation of the pixel level IR-window BT within the entire small box (2), the box-averaged cooling rate of remaining CTC pixels within the small box (1), and the maturity of the cloud types (1). A pixel with a sum of 'weight numbers' of 3 or more is determined to be marginally cooling/very immature and hence omitted. This admittedly can remove some vertically growing pixels at the very early stages of growth, however not all cooling clouds within

the very early stages of growth will mature into thunderstorms, so preference is given to keep the false alarm ratio as low as possible.

After all seven tests are completed, the final filtered CTC field is populated (Fig. 6). The majority of pixels within the unfiltered CTC (Fig. 4) product are eliminated since newly developing convective updrafts are very small spatially and are very uncommon compared to other cloud regimes (synoptic cloud systems, existing thunderstorm anvils, etc.).

Cooling pixels within the filtered CTC field are assigned a CI nowcast category based upon cloud top type trends. The UWCI nowcast is the final product of the algorithm and this is compared to the LI database in later sections. An example of the UWCI nowcast product is shown in Figure 7. Though this paper focuses on comparisons to LI events as a proxy for convective initiation, it is important to note the UWCI nowcasts from growing convective clouds can precede significant radar reflectivity. Over the northern Texas panhandle at 2015 UTC 29 April 2009 the first UWCI nowcast was made within an area of developing convective clouds (Fig. 7). At 2018 UTC the Amarillo, Texas base radar reflectivity shows no organized echoes over the northern Texas panhandle (Fig. 8). At 2035 UTC the radar reflectivity showed the first 35+ dBZ echoes associated with the developing storms in the northern Texas panhandle. Here, the UWCI nowcast offered a 20 min lead-time of the radar 35+ dBZ echoes. At 2103 UTC the radar reflectivity indicated intense precipitation with lightning initiation occurring at 2050 UTC and surface reports of large hail beginning near 2200 UTC (not shown). At 2018 UTC, other convection within the Amarillo radar range is evident to the southwest and southeast of the radar location. The convection southeast of the radar initiated earlier

than the 2015 UTC time examined in Figure 7 and hence no UWCI signal is present within that region at 2015 UTC. Additional convective development occurs to the southeast of the Amarillo radar after 2018 UTC and this growth was captured by the UWCI algorithm at 2032 UTC but is not shown in this example. The convection to the southwest of the Amarillo radar was developing and the UWCI algorithm indicated 'CI Occurring' in that area at 2015 UTC (Fig 7). The earliest indication of CI with the southwestern area of convection was at 1945 UTC (not shown).

In order to assign a UWCI nowcast, there must be at least 5 pixels with a filtered CTC of -4.0 K/15 min or less within the small box and there must be less than 5% thick ice pixels within the small box during the previous scan time. The minimum pixel requirement eliminates isolated pixels, ensuring a coherent signal when the product is visualized by an end-user. The -4.0 K/15 min threshold is a minimum CTC threshold described by Roberts and Rutledge (2003). The thick ice criteria ensure that only newly developing storms are assigned a nowcast; 5% or greater thick ice at the previous scan would signify a cloud that has confidently glaciated. The three UWCI nowcast categories consist of the following:

- Category 1 or 'Pre-CI Cloud Growth': At least 10% water cloud within the small box and less than 5% supercooled water, mixed phase, and thick ice at the current scan time. This category signifies clouds that are immature but exhibiting cooling due to vertical cloud growth. The results shown in the following section indicate that these Pre-CI Cloud Growth category pixels provide the highest nowcast lead-time for LI and/or significant radar echoes due to the relative immaturity of the clouds, but also have a higher false alarm ratio.

- Category 2 or 'CI Likely': At least 5% supercooled water or mixed phase cloud within the small box and less than 5% thick ice at the current scan time. This category identifies developing convective clouds that are beginning to exhibit early signs of glaciation. The CI Likely category provides a shorter lead-time than the Pre-CI Cloud Growth category, but also produces fewer false alarms because the developing clouds are more mature.
- Category 3 or 'CI Occurring': At least 5% thick ice within the small box at the current scan time. This category identifies convective clouds that have glaciated within the most recent satellite scan. This category offers the shortest nowcast lead time as these clouds the most mature and exhibits false alarm ratios similar to Category 2 nowcasts.

4. UWCI CI Nowcast Validation and Discussion

a) Validation Framework

The two metrics used to determine the accuracy of the UWCI nowcast fields are probability of detection (POD) and false alarm ratio (FAR). These statistics are generated by manually tracking clouds observed in GOES IR-window imagery, UWCI Nowcasts, and NLDN-derived LI events. Manual tracking was chosen instead of an automated method due to the temporal and spatial tracking and matching necessary to compute these accuracy statistics. Attempts for an automated system resulted in errant statistics, mainly due to 1) the significant distance that can be present between first CI nowcast and eventual LI location and 2) situations where multiple storms at varying stages of maturity occurring within a small area. An automated validation system would require

sophisticated object identification and tracking tools, which are currently under development at this time.

To compute POD, convective clouds for which LI has been found to occur are manually tracked back in time and space to determine if there was a CI nowcast associated with each LI event. If a match exists, the LI event is determined to have been correctly nowcast and the maximum lead-time and the associated CI nowcast category are recorded. Maximum lead-time refers to the earliest time a CI nowcast was made, as there can be a progression of CI nowcasts over multiple satellite scans for a given LI event. The POD is defined by the number correctly nowcast LI events divided by the total LI events in the database.

Figure 9 shows an example of how manual storm tracking was performed to determine POD at 2310 UTC on 25 April 2008. At 2310 UTC, LI is indicated over central Texas and northeastern Texas (cyan squares). Previous times show that UWCI nowcasts were associated with the central Texas LI event, but no nowcasts with the northeastern Texas LI event, thus the POD is 50% for this example. The central Texas LI event was correctly nowcast at 2232 UTC with a yellow (CI Likely) CI category and has 38 min lead-time.

A similar process is used to compute FAR. Clouds associated with all CI nowcasts for a given time are manually tracked forward in space and time to determine whether or not a LI event occurred at some point in the future. In this study, a cluster of nowcast pixels within a cloud is considered one CI nowcast, so the FAR calculations are not on an individual pixel basis. The false alarm ratio is defined as the total CI nowcasts minus correct CI nowcasts divided by the total CI nowcasts.

Figure 10 shows how manual storm tracking was performed to determine FAR at 1945 UTC on 29 April 2009. At 1945 UTC, CI nowcasts exist over the northern Texas Panhandle and over west-central Texas (red clusters). In this example the CI nowcast over west-central Texas was validated by an LI event at 1950 UTC, while the nowcast over the northern Texas panhandle does not have an associated LI event at any future time and is deemed a false alarm. In this example, the FAR at 1945 UTC is 50%. It should be noted that the manual tracking exceeds four consecutive scans, but four scans are shown for brevity in these POD and FAR examples.

The validation of the UWCI nowcast product covers 23 convective afternoons and 11 convective nights during April, May, June, and one night in July during 2008 and 2009 over the U.S. Central and Southern Plains. Two sets of POD and FAR statistics are generated. The first is for nowcasts covering the entire validation domain and the second covers areas enclosed by the "Slight Risk" region from the Storm Prediction Center 2000 UTC Day 1 Convective Outlook. The SPC Slight Risk region is introduced here to highlight UWCI nowcast performance in regions where hazardous thunderstorms are likely to form and be a focus for operational forecasting.

The afternoon validation time period is 1800 - 2359 UTC for POD and 1800 – 2245 UTC for FAR. The night validation time period is 0045 – 0615 UTC for POD and 0045 – 0545 UTC for FAR. The FAR window is smaller due to the nature of LI, which generally follows the time that a CI nowcast is made. If a CI nowcast were made at 2302 UTC, it would be tracked forward in space while searching for LI within this cloud until 2359 UTC. If no LI is found, it is possible this CI nowcast is indeed a false alarm, however, it is possible LI occurred sometime on the following day (defined by the 0000

UTC time). Since no false alarms are allowed after the 2245 UTC scan, any CI nowcasts that indeed validate within the 2300 UTC-hour cannot be counted as successful nowcasts, as the statistics would be biased toward successful nowcasts.

b) Validation Statistics

During the 23 convective afternoons and 11 convective nights, there are 487 LI events within the entire validation domain, 341 of those events fall within the SPC risk area. There are 509 CI nowcasts within the entire validation domain, 380 of those events fall within the SPC risk area. The POD and FAR statistics are 47.0% and 34.8% over the entire validation domain. For the regions enclosed by a SPC slight or greater risk region, the mean statistics improve to 56.3% for POD and 25.5% for FAR. These statistics show that: 1) the UWCI algorithm is less likely to successfully nowcast convection away from regions of expected severe weather than within regions of expected severe weather and 2) there is a higher probability of false alarm away from regions of expected severe weather than within regions of expected severe weather. Based upon the cases sampled here, these statistics imply that a forecaster can assume that slightly more than half of CG lightning producing storms within an SPC risk area will be successfully nowcast and that roughly 3 of every 4 clouds with CI nowcasts will produce lightning at some point in the future, which in this study is a proxy for convective initiation. Given that operational weather forecasters can skillfully predict the general area of expected severe convection (Ostby, 1999), the UWCI nowcasts can pinpoint where convection will develop within these forecasted risk areas. Details of such nowcasts are examined in the following subsection.

c) Discussion

The mean statistics described previously do not account for the variability of the POD and FAR between convective days. Tables 1 (daytime) and 2 (nighttime) show the POD and FAR for each day within the validation dataset. It is clear that the validation statistics can vary significant across convective events. Periods with POD greater than one standard deviation above the mean (day: 8 May 2009, 13 May 2009, 15 May 2009, 26 May 2009, and 12 June 2009; night: 13 June 2009, 16 July 2009, and 01 June 2008) featured storms that developed in areas absent of existing convective anvils or cirrus canopies and were generally along cold fronts/dry lines. Periods with POD greater than one standard deviation below the mean (day: 6 May 2009, 12 May 2009, and 24 May 2008; night: 16 June 2009, 24 May 2008, and 27 May 2008) generally featured fast storm motion, mid to upper level cloud layers, and/or existing anvils that obscured storms with new LI.

The periods with FAR greater than one standard deviation above the mean consisted of one day with a very small sample size (2 storms, 6 May 2009) and four periods (day: 17 June 2009 and 29 April 2009; night: 01 May 2009 and 30 May 2008) had developing convective towers that showed vertical development but later dissipated prior to producing CG lightning or that exhibited fast storm motion. Periods with FAR less than one standard deviation below the mean generally were very "clean" days, meaning that convection developed from clear skies along cold fronts/dry lines and had moderate to large sample sizes (10, 20, and 13 on days 28 June 2009, 26 May 2008, and 27 May 2008, respectively (all daytime)). The breakdown of these extreme days allow forecasters to know when the algorithm can be expected to perform very well (slower

moving storms developing along sharp boundaries in absence of debris or other surrounding clouds) and when the algorithm may struggle (fast cloud/storm motion or the presence of obscuring debris clouds).

For the successfully nowcasted events, it is possible to determine the lead time prior to LI provided by the earliest UWCI nowcast for each nowcast category. As stated in Section 3b, the Pre-CI Cloud Growth nowcast category offers the longest lead time, most commonly > 60 min ahead of LI (Fig. 11). The CI Likely category most often offers moderate lead-time for LI (31-45 min). The CI Occurring category most often offers the shortest lead-time (0-15 min). The progression of lead time by nowcast type is rather intuitive in that the most immature developing convective clouds recognized by the UWCI algorithm offer the longest lead-times, while developing mature clouds that have established thick cloud tops offer the shortest lead-times. Lead-times of less than zero minutes represent situations when the first CI nowcast occurs shortly after LI. The 13 to 17 minute temporal resolution of GOES, as well as the 30-minute full-disk scan gaps are largely to blame in these cases. Sub-zero minute lead-time events are still included in the statistics as these are a function of the satellite technology, not the methodology or underlying science. The UWCI algorithm can, and in our real-time processing does, take advantage of the rapid scan operations of current GOES. Future imagers, such as ABI offer much promise with an expected 5-minute refresh rate over CONUS and even higher refresh rates over select 'mesoscale' domains (Schmit et al. 2005).

The percentage of false alarms by UWCI nowcast category was also determined for the SPC slight risk or greater regions. For the 380 CI nowcasts, the total breakdown by category was the following: 44 Pre-CI Cloud Growth, 75 CI Likely, and 261 CI

Occurring. The percentage of false alarm by category was as follows: 43% Pre-CI Cloud Growth, 20% CI Likely, and 24% CI Occurring. These results suggest that newly developing convective clouds exhibit a higher FAR than clouds at later stages of growth. This result is expected since developing convective clouds with supercooled, mixed phased, and/or ice tops are already closer to the mature thunderstorm phase (and also nearer to producing CG lightning strikes) than warm, water clouds which do not always evolve into thunderstorms even if they show some vertical growth signal.

5. Conclusions

Convective storms have direct impact on the economy, personal property, and personal health, and safety. Prediction of exact time and location of convective storms remains a challenge for operational forecasters and numerical weather prediction. The rapid refresh rate (5 to 15 min) of geostationary imagers provides an opportunity to devise an algorithm using infrared measurements to monitor convective cloud growth and nowcast convective initiation with up to one-hour lead-times.

The algorithm described in this text, the University of Wisconsin Convective Initiation (UWCI) nowcast utilizes a box-averaged approach for monitoring cloud top cooling rates. The UWCI approach has advantages over existing methodologies. It is computationally inexpensive, uses a physically based IR-only cloud type algorithm allowing day/night independence, and is portable from one geostationary imager platform to another. The UWCI algorithm separates false cloud top cooling associated with horizontal cloud advection from true cloud top cooling associated with vertical cloud growth through a series of tests. After the true cloud top cooling signal is isolated, the

cooling pixels are assigned convective initiation nowcast categories based upon cloud top type classification and trends. Three categories exist, Pre-CI Cloud Growth, CI Likely, and CI Occurring, which represent vertically growing water cloud, vertically growing supercooled/mixed phase cloud, and vertically growing, recently glaciated cloud, respectively.

In this study, lightning initiation (LI) derived from the National Lightning Detection Network cloud-to-ground (CG) strikes serves as a proxy for convective initiation. The validation consists of manually tracking clouds through space and time using GOES-12 IR-window imagery to determine: 1) the LI probability of detection (POD), which is defined as the number of LI events within the validation period that were correctly nowcast by the UWCI algorithm and 2) the UWCI nowcast false alarm ratio (FAR), which is defined as the number of UWCI nowcasts that were not associated with an LI event. The validation study focused on the Storm Prediction Center severe storm risk areas for 23 convective afternoons and 11 convective nights over the Southern and Central Plains during April, May, June, and one night in July during 2008 and 2009. Within the SPC severe storm risk area, the mean POD is 56.3% and the mean FAR is 25.5% (47.0% POD and 34.8% FAR for entire validation domain). Analysis of the outlying days with POD/FAR above or below one standard deviation of the respective mean reveals that the UWCI algorithm performs 1) better in certain regimes such as with storms developing in previously clear to partly cloudy skies and with storm development along sharp boundaries and 2) poorer in other regimes such as scenes covered with mid-level cloud layers, cirrus shields, existing convective anvils, and fast cloud motion. The analysis showed the “pre-CI cloud growth” nowcast category offers the largest lead-times

of the three nowcast categories, but also has a highest FAR. The "CI Likely" and "CI Occurring" nowcast categories show progressively shorter lead-times, respectively. The lead-times grow shorter with the CI Likely and CI Occurring categories since these nowcasts are capturing developing convection further along in the development process lifecycle, but have similarly lower FAR.

The UWCI algorithm is a decision support tool currently being evaluated by Storm Prediction Center personnel, National Weather Service Forecast Office personnel, and NOAA Satellite Analysis Branch personnel with goals of improving convective nowcasting in the 0-1 hour time frame. The feedback cycle between operations and researchers is crucial for improving algorithm, visualization, and forecasts**.**

6. Acknowledgements

The authors would like to thank the Space Science and Engineering Center (SSEC) data center for support in acquiring data, Russ Schneider and Chris Siewert at the Storm Prediction Center (SPC) and Jeff Craven and the forecasting team at the Milwaukee/Sullivan National Weather Service Forecast Office for evaluation of the UWCI algorithm and providing critical feedback. This research is supported by NOAA GOES Product Assurance Plan (GIMPAP) award NA06NES4400002.

7. References

Bedka, K.M. and J.R. Mecikalski, 2005: Application of satellite-dervied atmospheric motion vectors for estimating mesoscale flows. *J. Appl. Meteo.*, **44**, 1761-1772.

Bedka, K.M., C.S. Velden, R.A. Petersen, W.F. Feltz, and J.R. Mecikalski, 2009: Comparisons of Satellite-Derived Atmospheric Motion Vectors, Rawinsondes, and NOAA Wind Profiler Observations. *J. Appl. Meteor.,* **48**, 1542-1561.

Berendes, T. A., J. R. Mecikalski, W. M. MacKenzie, K. M. Bedka, and U. S. Nair, 2008: Convective cloud identification and classification in daytime satellite imagery using standard deviation limited adaptive clustering. *J. Geophys. Res*., **113**, (d20): D20207.

Browning, K.A., A.M. Blyth, P.A. Clark, U. Corsmeier, C.J. Morcrette, J.L. Agnew, S.P. Ballard, D. Bamber, C. Barthlott, L.J. Bennett, K.M. Beswick, M. Bitter, K.E. Bozier, B.J. Brooks, C.G. Collier, F. Davies, B. Deny, M.A. Dixon, T. Feuerle, R.M. Forbes, C. Gaffard, M.D. Gray, R. Hankers, T.J. Hewison, N. Kalthoff, S. Khodayar, M. Kohler, C. Kottmeier, S. Kraut, M. Kunz, D.N. Ladd, H.W. Lean, J. Lenfant, Z. Li, J. Marsham, J. McGregor, S.D. Mobbs, J. Nicol, E. Norton, D.J. Parker, F. Perry, M. Ramatschi, H.M.A. Ricketts, N.M. Roberts, A. Russell, H. Schulz, E.C. Slack, G. Vaughan, J. Waight, D.P. Wareing, R.J. Watson, A.R. Webb, and A. Wieser, 2007: The Convective Storm Initiation Project. *Bull. Amer. Meteor. Soc.*, **88**, 1939–1955.

Carvalho, L.M.V., and C. Jones, 2001: A Satellite Method to Identify Structural Properties of Mesoscale Convective Systems Based on the Maximum Spatial Correlation Tracking Technique (MASCOTTE). *J. Appl. Meteor.*, **40**, 1683–1701.

Cummins, K.L., M.J. Murphy, E.A. Bardo, W.L. Hiscox, R.B. Pyle and A.E. Pifer, 1998: A combined TOA/MDF technology upgrade of the U.S. National Lightning Detection Network. *J. Geophys. Res.*, **103**, 9035-9044.

Demetriades, N.W.S., M.J. Murphy, and R.L. Holle, 2004: The importance of total lightning in the future of weather nowcasting. *Symposium on Planning, Nowcasting, and Forecasting in the Urban Zone, AMS Annual Meeting*, 12 January 2004, Seattle, Washington.

Dye, J.E., W.P. Winn, J.J. Jones, and D.W. Breed, 1989: The Electrification of New Mexico Thunderstorms. 1. Relationship Between Precipitation Development and the Onset of Electrification. *J. Geophys. Res.*, **94**, 8643-8656.

Goodman, S.J., R. Blakeslee, W. Koshak, W.A. Petersen, L. Carey, and D. Mach, 2010: The Geostationary Lightning Mapper (GLM) for GOES-R: A new operational capability to improve storm forecasts and warnings. *6th Annual Symposium on Future National Operational Environmental Satellite Systems, AMS Annual Meeting*, 20 January 2010, Atlanta, Georgia.

Goodman, S.J., R. Blakeslee, H. Christian, W. Koshak, J. Bailey, J. Hall, E. McCaul, D. Buechier, C. Darden, J. Burks, T. Bradshaw, and P. Gatlin, 2005: The North Alabama Lightning Mapping Array: Recent severe storm observations and future prospects. *Atmospheric Research*, **76**, 423-437.

Goodman, S.J., D.E. Buechler, and P.J. Meyer, 1988: Convective Tendency Images Dervied from a Combination of Lightning and Satellite Data. *Wea. Forecasting*, **3**, 173-188.

Heidinger, A.K., 2010: ABI Cloud Mask Algorithm Theoretical Basis Document. NOAA NESDIS Center for Satellite Applications and Research (STAR), 67 pp.

Iskenderian, H., John R. Mecikalski, Wayne M. MacKenzie Jr., Wayne F. Feltz, Kristopher M. Bedka, 2009: Using Satellite Data to Improve Convective Forecasts in the Collaborative Storm Prediction for Aviation (CoSPA). *1st American Institute of Aeronautics and Astronautics Atmospheric and Space Environments Conference*, San Antonio, TX.

Johns, R.H., and C.A. Doswell III, 1992: Severe local storms forecasting. *Wea. Forecasting*, **7**, 588-612.

Johnson, D.B., P. Flament, and R.L. Bernstein, 1994: High-Resolution Satellite Imagery for Mesoscale Meteorological Studies. *Bull. Amer. Meteor. Soc.*, **75**, 5–33.

Kaplan,M.L., Y-L. Lin, A.J. Riordan, K.T.Waight, K.M. Lux, and A.W. Huffman, 1999: Flight safety characterization studies, part I: turbulence categorization analyses. *Interim Subcontrator Report to Research Triangle Institute*, NASA contract NAS1-99074.

Koenig M, and E. de Coning, 2008: The MSG Global Instability Indices Product and its Use as a Nowcasting Tool. *Wea. Forecasting*., **24**, 272-285.

Lakshmanan, V., T. Smith, G.J. Stumpf, and K. Hondi, 2007: The warning decision support system – integrated information. *Wea. Forecasting*, **22**, 596-612.

Machado, L.A.T., and H. Laurent, 2004: The Convective System Area Expansion over Amazonia and Its Relationships with Convective System Life Duration and High-Level Wind Divergence. *Mon. Wea. Rev.*, **132**, 714–725.

Maddox, R.A., 1980: Mesoscale convective complexes. *Bull. Amer. Meteor. Soc.*, **61**,1374–1387.

Mecikalski, J.R., and K.M. Bedka, 2006: Forecasting Convective Initiation by Monitoring the Evolution of Moving Cumulus in Daytime GOES Imagery. *Mon. Wea. Rev.*, **134**, 49–78.

Mecikalski, J.R., K. Bedka, S. Paech, and L. Litten, 2008: A statistical evaluation of GOES cloud-top properties for nowcasting convective initiation. *Mon. Wea. Rev.,* **136**, 4899-4914.

Mecikalski, J. R., J. J. Murray, W. F. Feltz, D. B. Johnson, K. M. Bedka, S. M. Bedka, A. Wimmers, M. Pavolonis, T. Berendes, J. Haggerty, P. Minnis, B. Bernstein, and E. Williams, 2007: Aviation applications for satellite based observations of cloud properties, convective initiation, in-flight icing, turbulence and volcanic ash. *Bull Amer. Meteor. Soc*. **88**, 1589-1607.

Menzel, W.P. and J.F.W. Purdom, 1994: Introducing GOES-I: The First of a New Generation of Geostationary Operational Environmental. *Bull. Amer. Meteor. Soc.,* **75**, 757-781.

Moller, A.R., 2001: Severe local storms forecasting. *Severe Convective Storms, Meteor. Monogr*., **50**, American Meteorological Society, 433-480.

Morel, C. S. Senesi, and F. Autones, 2000: Building upon SAF-NWC products: Use of the Rapid Developing Thunderstorms (RDT) product in Meteo-France nowcasting tools. *The 2002 Meteorological Satellite Data Users' Conference*, Eumetsat and Met Eirean, Dublin, Ireland, 248-255.

Murray, J. J., 2002: Aviation weather applications of Earth Science Enterprise data. *Earth Observing Magazine*, **11**, No. 8, pp. 26-30.

Otsby, F.P., 1999: Improved Accuracy in Severe Storm Forecasting by the Severe Local Storms Unit during the Last 25 Years: Then versus Now. *Wea. Forecasting*, **14**, 526-543.

Pavolonis, M.J, 2010a: Advances in extracting cloud composition from spaceborne radiances: A robust alternative to brightness temperatures, Part I: Theory. *J. Appl. Meteor. Climatol*, In Press.

Pavolonis, M.J, 2010b: ABI Cloud Type/Phase Algorithm Theoretical Basis Document. NOAA NESDIS Center for Satellite Applications and Research (STAR), 60 pp.

Pavolonis, M.J. and A.K. Heidinger, 2004: Daytime Cloud Overlap Detection from AVHRR and VIIRS. *J. Appl. Meteor.*, **43**, 762-778.

Pavolonis, M.J., A.K. Heidinger, and T. Uttal, 2005: Daytime Global Cloud Typing From AVHRR and VIIRS: Algorithm Description, Validation, and Comparisons. *J. Atmos. Oceanic Technol.*, **44**, 804-826.

Rabin, R. M., and T. Whittaker, 2006: Tool for Storm Analysis Using Multiple Data Sets. Advances in Visual Computing, G. Bebis, R. Boyle, D. Koracin, B. Parvin, Ed(s)., Springer, 571-578.

Rison, W., R.J. Thomas, P.R. Krehbiel, T. Hamlin, and J. Harlin, 1999: A GPS-based three-dimensional lightning mapping system: initial observations in central New Mexico. *Geophys. Res. Lett.*, **26**, 3573-3576.

Roberts, R.D., and S. Rutledge, 2003: Nowcasting Storm Initiation and Growth Using *GOES-8* and WSR-88D Data. *Wea. Forecasting*, **18**, 562–584.

Schmit, T. J., M. M. Gunshor, W. P. Menzel, J. Li, S. Bachmeier, and J. J. Gurka, 2005: Introducing the Next-generation Advanced Baseline Imager (ABI) on GOES-R. *Bull. Amer. Meteor. Soc.*, **86**, 1079-1096.

Vila, D.A., L.A.T. Machado, H. Laurent, and I. Velasco, 2008: Forecast and Tracking the Evolution of Cloud Clusters (ForTraCC) Using Satellite Infrared Imagery: Methodology and Validation. *Wea. Forecasting*, **23**, 233–245.

Wagner T. J., W. F. Feltz, and S. A. Ackerman, 2008: The temporal evolution of convective indices in storm-producing environments. *Wea. Forecasting*, **23**, 786-794.

Zinner, T., H. Hammstein, and A. Tafferner, 2008: Cb-TRAM: Tracking and monitoring severe convection from onset over rapid development to mature phase using multi-channel Meteosat-8 SEVIRI data. *Meteor. Atmos. Phys.,* **101**, 191-210.

Figure Caption List

Figure 1. Example of improved version of Pavolonis et al. 2005 cloud type algorithm for 2015 UTC 29 April 2009 (left) and corresponding false color image (right) red: 0.65 μm reflectance, green: 3.9 μm reflectance, and blue 11 μm brightness temperature.

Figure 2. Binned 5-minuted lightning plot valid at 2040 UTC 29 April 2009. The current time (0 min since current) is plotted in red. Previous 5-minute lightning bins are plotted in various colors depending on the age of the lightning strikes. Lightning Initiation is occurring at the location highlighted by the red circle.

Figure 3. Box-averaged GOES-12 IR-Window Brightness Temperature valid 2015 UTC 29 Apr 2009 (left) and native satellite resolution IR-Window Brightness Temperature valid at the same time (right). Black areas in the left panel reflect missing values (e.g.-areas where there are insufficient cloudy pixels to compute a box-average BT.)

Figure 4. Unfiltered CTC rate [K / 15 min] valid at 2015 UTC on 29 Apr 2009. The unfiltered product contains true cooling due to vertical cloud growth and false cooling due to horizontal cloud advection. White areas represent missing values (e.g.-no cooling was present).

Figure 5. Flow chart of UWCI algorithm steps. Seven tests are utilized for filtering false cloud-top cooling and are described within the text.

Figure 6. Filtered CTC rate [K / 15 min] valid at 2015 UTC on 29 April 2009. The filtered CTC are determined to be portions of the unfiltered CTC (Fig. 4) due to vertical cloud growth, not horizontal advection. White areas represent missing values (e.g.-where cooling was filtered or where no cooling was initially present).

Figure 7. Example of UWCI nowcast valid 2015 UTC 29 April 2009. In this example CI nowcasts were made over the Texas panhandle and southwestern Kansas.

Figure 8. Top panel shows Amarillo, Texas radar base reflectivity at 2018 UTC 29 April 2009, middle panel shows radar reflectivity at 2035 UTC, and bottom panel shows radar reflectivity at 2103 UTC. The yellow circle corresponds to areas of UWCI nowcasts made at 2015 UTC (Fig. 7). The first 35+ dBZ radar reflectivity with newly developing storms occurs at 2035 UTC, or 20 min after the first UWCI nowcast. Radar reflectivity by 2103 UTC shows intense radar echoes with storms later producing surface severe weather reports (not shown).

Figure 9. The four-panel image demonstrates how LI events are validated for probability of detection statistics. The underlying imagery is GOES-12 IR-window BT. The green, yellow, and red objects indicate UWCI nowcasts for Pre-CI Cloud Growth, CI Likely, and CI Occurring nowcast categories, respectively. The cyan squares indicate LI locations for the time indicated within the 'LI:' label. The top left panel shows LI valid at 2310 UTC on 25 April 2008 with underlying satellite imagery and UWCI nowcasts at

2302 UTC. The remaining panels show satellite imagery and UWCI nowcasts for previous satellite scans (no LI occurred at these times).

Figure 10. The four-panel image demonstrates how LI events are validated for false alarm ratio statistics. The underlying imagery is GOES-12 IR-Window Brightness Temperature. The green, yellow, and red objects indicate UWCI nowcasts for Pre-CI Cloud Growth, CI Likely, and CI Occurring nowcast categories, respectively. The cyan squares indicate LI locations for the time indicated within the 'LI:' label. The top left panel shows LI valid at 1950 UTC 29 April 2009 with underlying satellite imagery and UWCI nowcasts at 1945 UTC. The remaining panels show satellite imagery and UWCI nowcasts for subsequent satellite scans (no LI occurred at these times).

Figure 11. Relative frequency of lead-time by UWCI nowcast category for all successfully nowcast LI events within SPC slight risk or greater regions. Green bars reflect Pre-CI Cloud Growth, yellow bars reflect CI likely category, and red reflect CI occurring category.

Table 1. Probability of Detection (POD), False Alarm Ratio (FAR), Lightning Initiation (LI) count, and Nowcast count statistics for SPC Slight Risk or greater region for 23 convective afternoons within the validation dataset.

Day	POD	FAR	LI Count	Nowcast Count
16 Apr 2009	38%	12%	26	17
29 Apr 2009	67%	48%	12	21
06 May 2009	25%	50%	4	2
08 May 2009	100%	14%	3	7
12 May 2009	25%	38%	12	8
13 May 2009	86%	20%	7	10
15 May 2009	80%	8%	15	24
20 May 2009	75%	30%	4	10
26 May 2009	100%	14%	2	7
31 May 2009	65%	13%	17	16
12 Jun 2009	86%	25%	7	12
17 Jun 2009	58%	53%	12	19
26 Jun 2009	50%	40%	6	5
27 Jun 2009	52%	0%	19	13
25 Apr 2008	73%	29%	11	14
26 Apr 2008	50%	38%	8	8
10 May 2008	55%	13%	11	8
22 May 2008	40%	30%	15	10
23 May 2008	64%	40%	11	15
24 May 2008	25%	25%	8	4
25 May 2008	65%	42%	17	33
26 May 2008	50%	6%	20	17
28 May 2008	38%	0%	13	8
Mean/Std. Dev	55.4% / 22.2%	26.0% / 16.0%	-	-
Sum	-	-	260	288

Table 2. Probability of Detection (POD), False Alarm Ratio (FAR), Lightning Initiation (LI) count, and Nowcast count statistics for SPC Slight Risk or greater region for 11 convective nights within the validation dataset.

Day	POD	FAR	LI Count	Nowcast Count
01 May 2009	50%	73%	6	11
08 Jun 2009	50%	10%	10	10
11 Jun 2009	67%	0%	6	8
13 Jun 2009	83%	13%	6	8
16 Jun 2009	33%	0%	6	2
16 Jul 2009	83%	0%	6	8
24 May 2008	40%	0%	5	2
27 May 2008	40%	25%	5	4
30 May 2008	71%	56%	7	16
01 Jun 2008	80%	15%	10	13
28 Jun 2008	50%	0%	14	10
Mean/Std. Dev	59.3% / 18.6%	23.9% / 25.0%	-	-
Sum	-	-	81	92

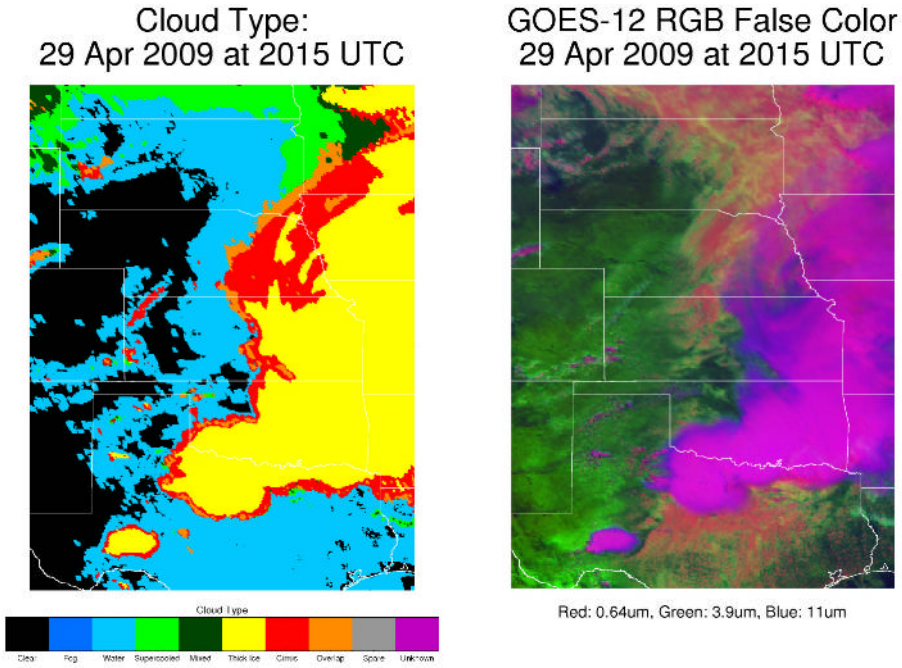

Figure 1. Example of improved version of Pavolonis et al. 2005 cloud type algorithm for 2015 UTC 29 April 2009 (left) and corresponding false color image (right) red: 0.65 µm reflectance, green: 3.9 µm reflectance, and blue 11 µm brightness temperature.

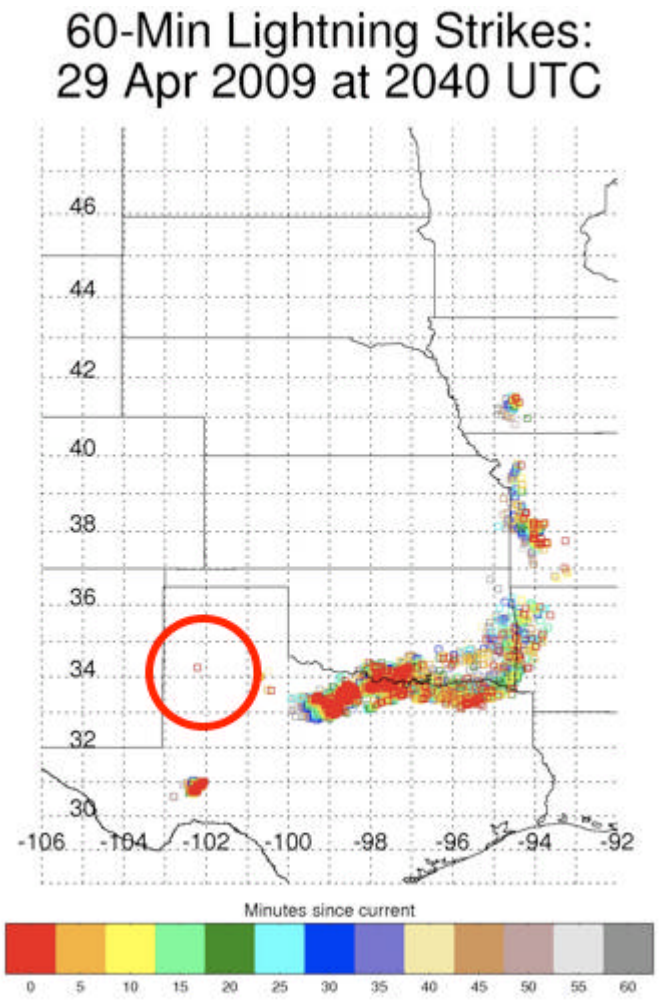

Figure 2. Binned 5-minuted lightning plot valid at 2040 UTC 29 April 2009. The current time (0 min since current) is plotted in red. Previous 5-minute lightning bins are plotted in various colors depending on the age of the lightning strikes. Lightning Initiation is occurring at the location highlighted by the red circle.

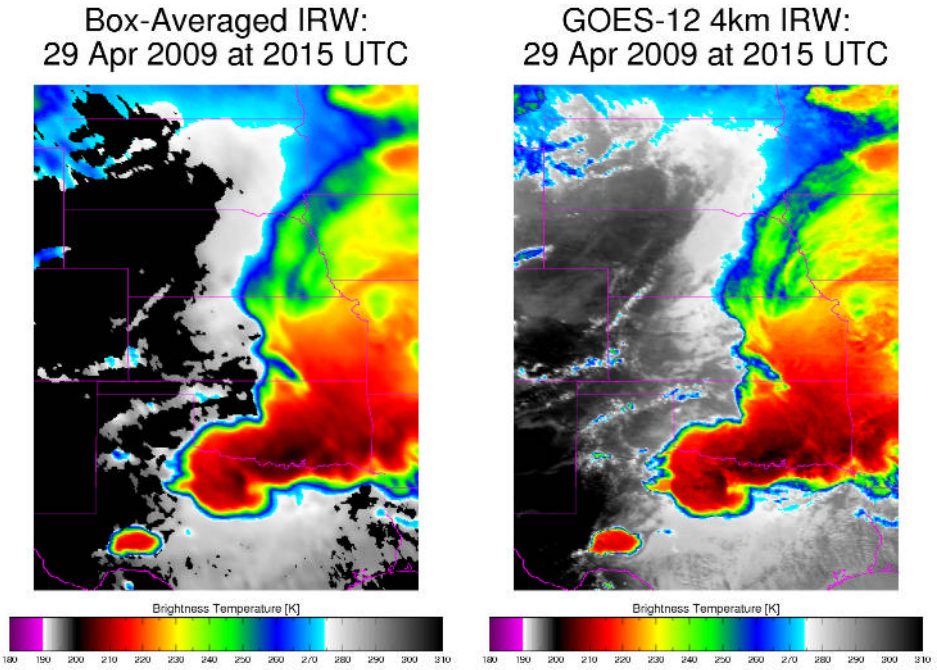

Figure 3. Box-averaged GOES-12 IR-Window Brightness Temperature valid 2015 UTC 29 Apr 2009 (left) and native satellite resolution IR-Window Brightness Temperature valid at the same time (right). Black areas in the left panel reflect missing values (e.g.- areas where there are insufficient cloudy pixels to compute a box-average BT.)

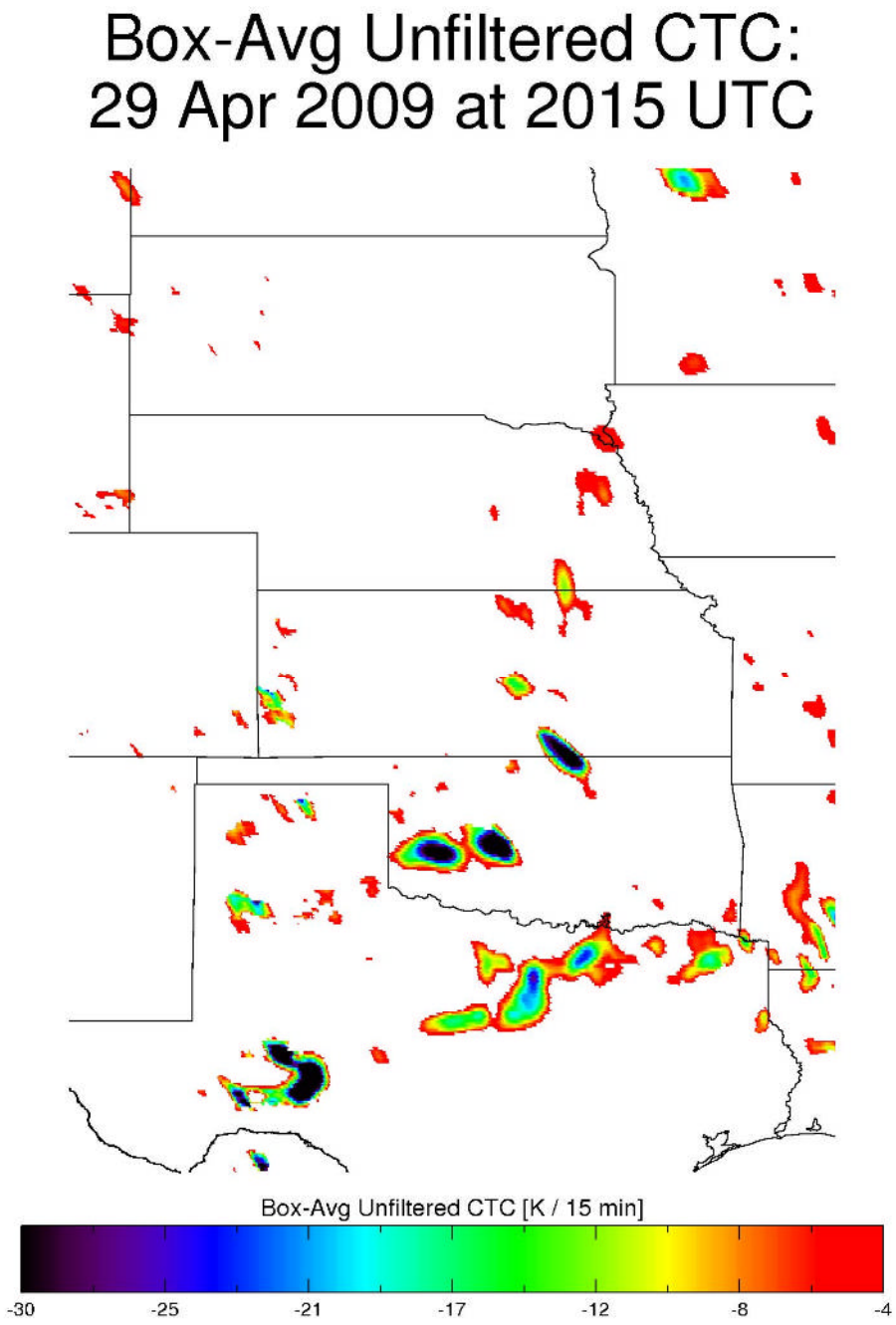

Figure 4. Unfiltered CTC rate [K / 15 min] valid at 2015 UTC on 29 Apr 2009. The unfiltered product contains true cooling due to vertical cloud growth and false cooling due to horizontal cloud advection. White areas represent missing values (e.g.-no cooling was present).

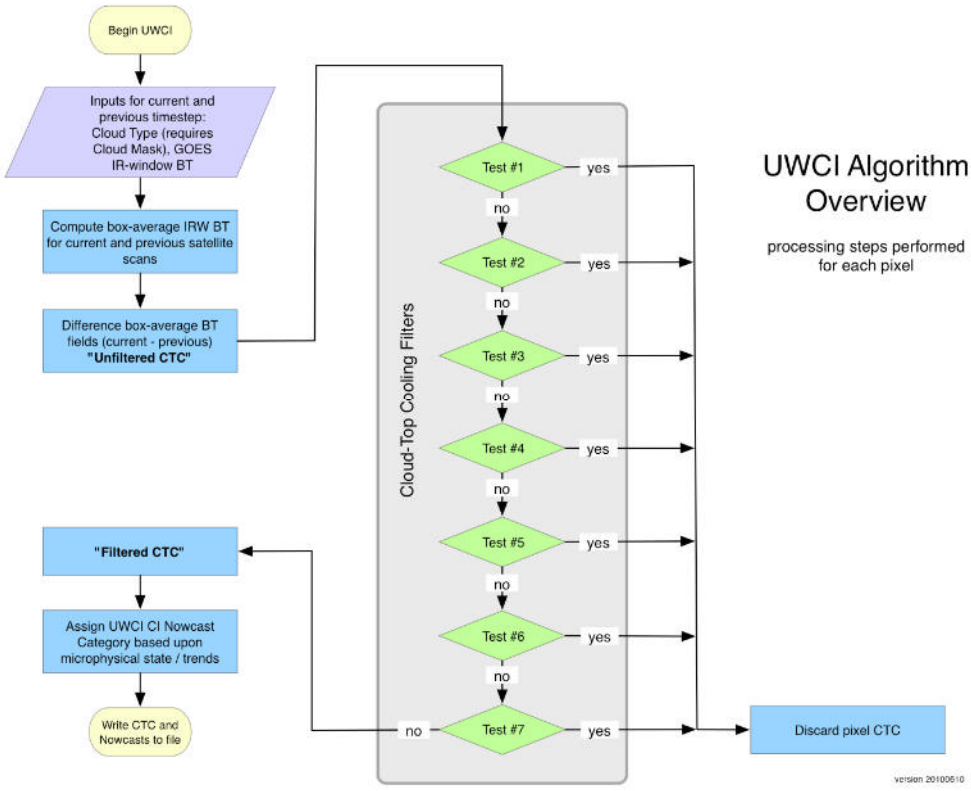

Figure 5. Flow chart of UWCI algorithm steps. Seven tests are utilized for filtering false cloud-top cooling and are described within the text.

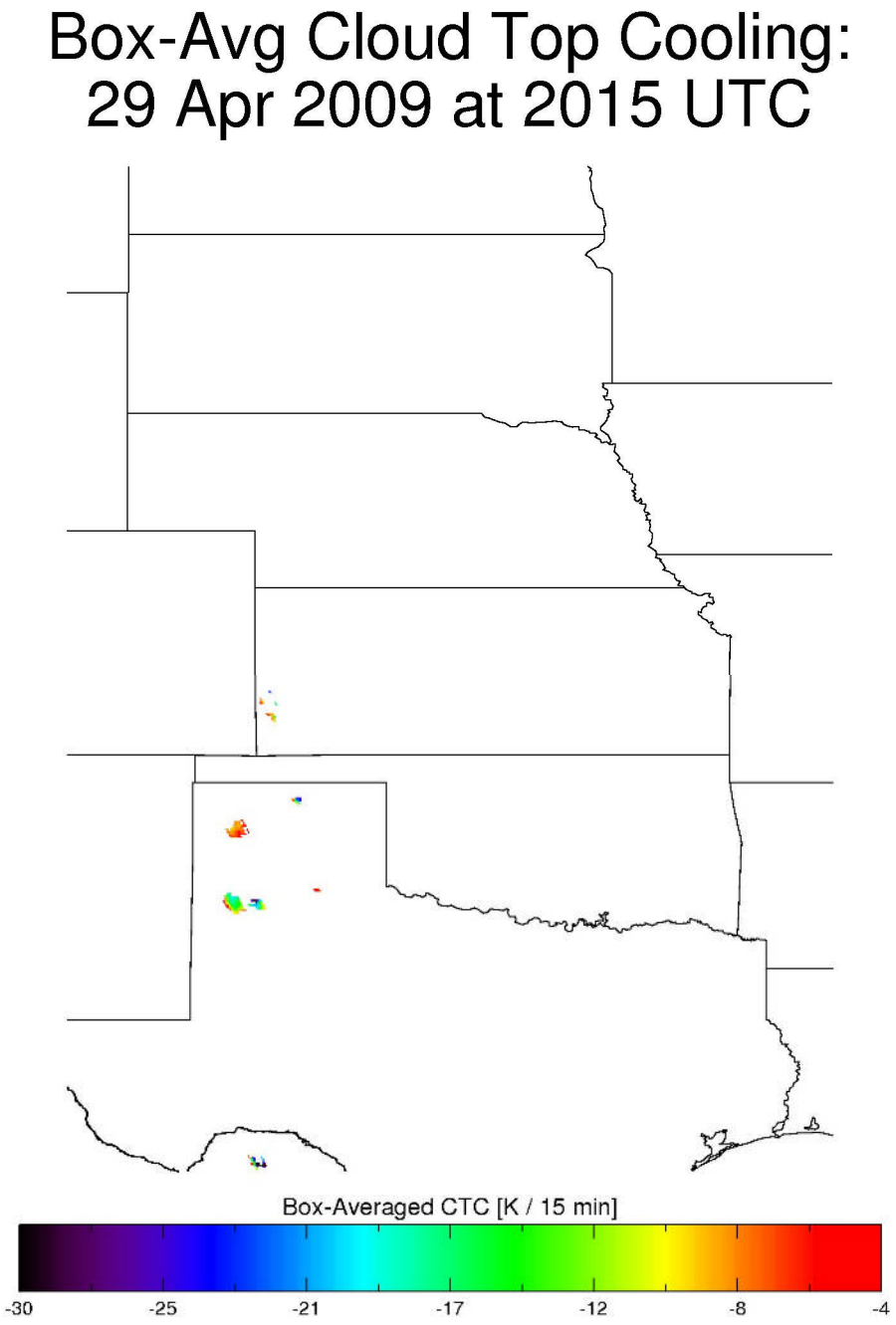

Figure 6. Filtered CTC rate [K / 15 min] valid at 2015 UTC on 29 April 2009. The filtered CTC are determined to be portions of the unfiltered CTC (Fig. 4) due to vertical cloud growth, not horizontal advection. White areas represent missing values (e.g.-where cooling was filtered or where no cooling was initially present).

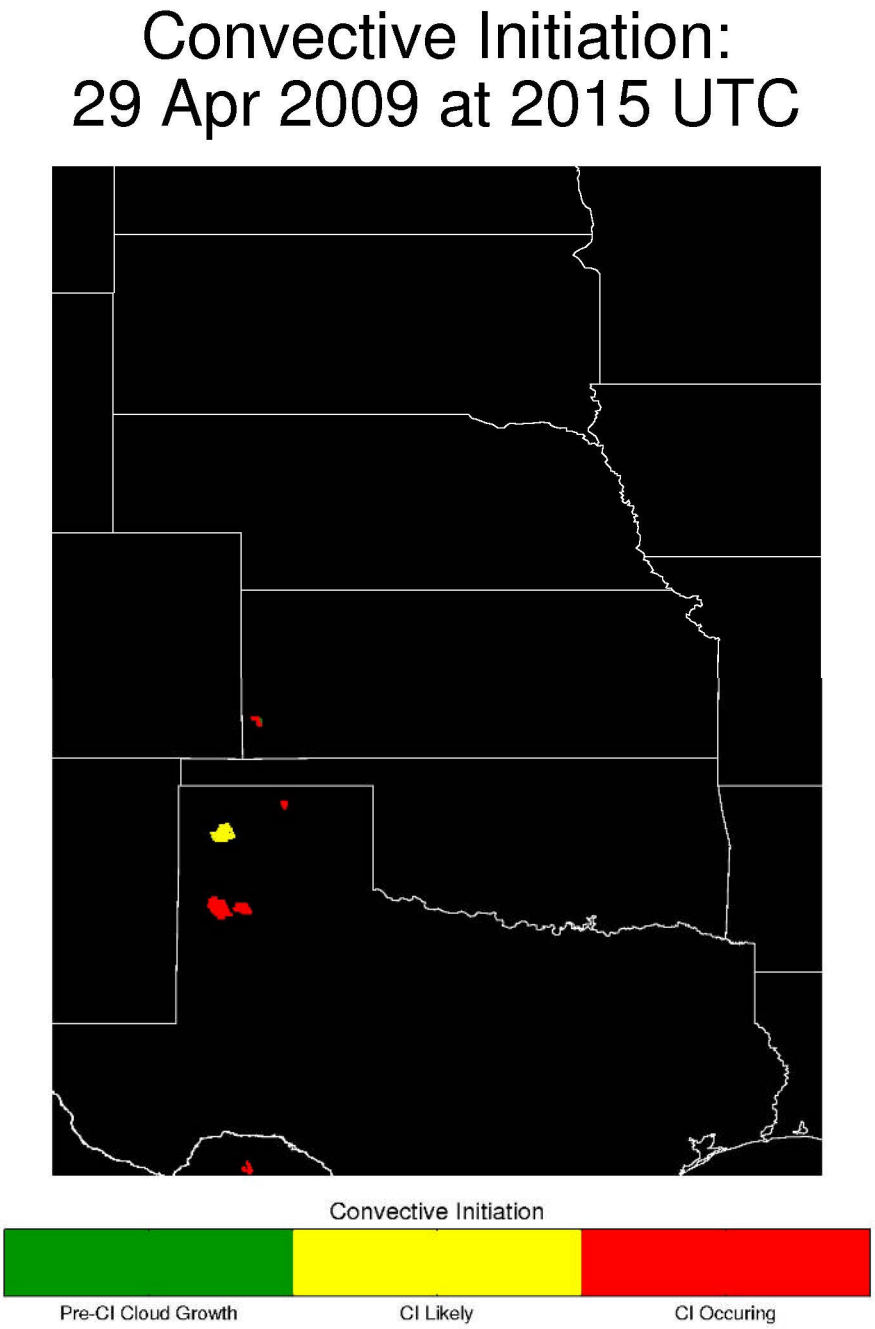

Figure 7. Example of UWCI nowcast valid 2015 UTC 29 April 2009. In this example CI nowcasts were made over the Texas panhandle and southwestern Kansas.

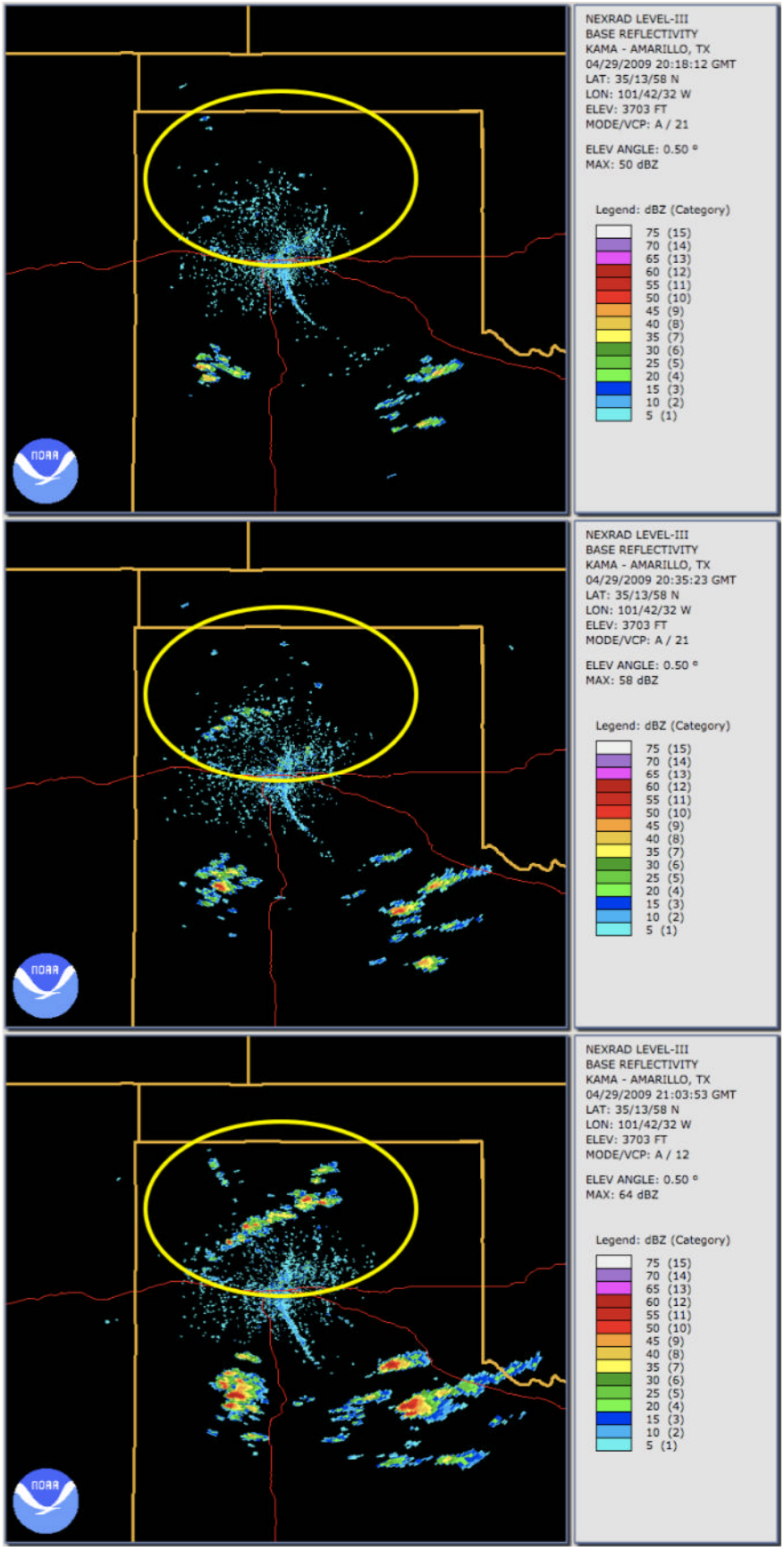
NEXRAD LEVEL-III
BASE REFLECTIVITY
KAMA - AMARILLO, TX
04/29/2009 20:18:12 GMT
LAT: 35/13/58 N
LON: 101/42/32 W
ELEV: 3703 FT
MODE/VCP: A / 21
ELEV ANGLE: 0.50 °
MAX: 50 dBZ
Legend: dBZ (Category)
75 (15)
70 (14)
65 (13)
60 (12)
55 (11)
50 (10)
45 (9)
40 (8)
35 (7)
30 (6)
25 (5)
20 (4)
15 (3)
10 (2)
5 (1)
NEXRAD LEVEL-III
BASE REFLECTIVITY
KAMA - AMARILLO, TX
04/29/2009 20:35:23 GMT
LAT: 35/13/58 N
LON: 101/42/32 W
ELEV: 3703 FT
MODE/VCP: A / 21
ELEV ANGLE: 0.50 °
MAX: 58 dBZ
Legend: dBZ (Category)
75 (15)
70 (14)
65 (13)
60 (12)
55 (11)
50 (10)
45 (9)
40 (8)
35 (7)
30 (6)
25 (5)
20 (4)
15 (3)
10 (2)
5 (1)
NEXRAD LEVEL-III
BASE REFLECTIVITY
KAMA - AMARILLO, TX
04/29/2009 21:03:53 GMT
LAT: 35/13/58 N
LON: 101/42/32 W
ELEV: 3703 FT
MODE/VCP: A / 12
ELEV ANGLE: 0.50 °
MAX: 64 dBZ
Legend: dBZ (Category)
75 (15)
70 (14)
65 (13)
60 (12)
55 (11)
50 (10)
45 (9)
40 (8)
35 (7)
30 (6)
25 (5)
20 (4)
15 (3)
10 (2)
5 (1)

Figure 8. Top panel shows Amarillo, Texas radar base reflectivity at 2018 UTC 29 April 2009, middle panel shows radar reflectivity at 2035 UTC, and bottom panel shows radar reflectivity at 2103 UTC. The yellow circle corresponds to areas of UWCI nowcasts made at 2015 UTC (Fig. 7). The first 35+ dBZ radar reflectivity with newly developing storms occurs at 2035 UTC, or 20 min after the first UWCI nowcast. Radar reflectivity by 2103 UTC shows intense radar echoes with storms later producing surface severe weather reports (not shown).

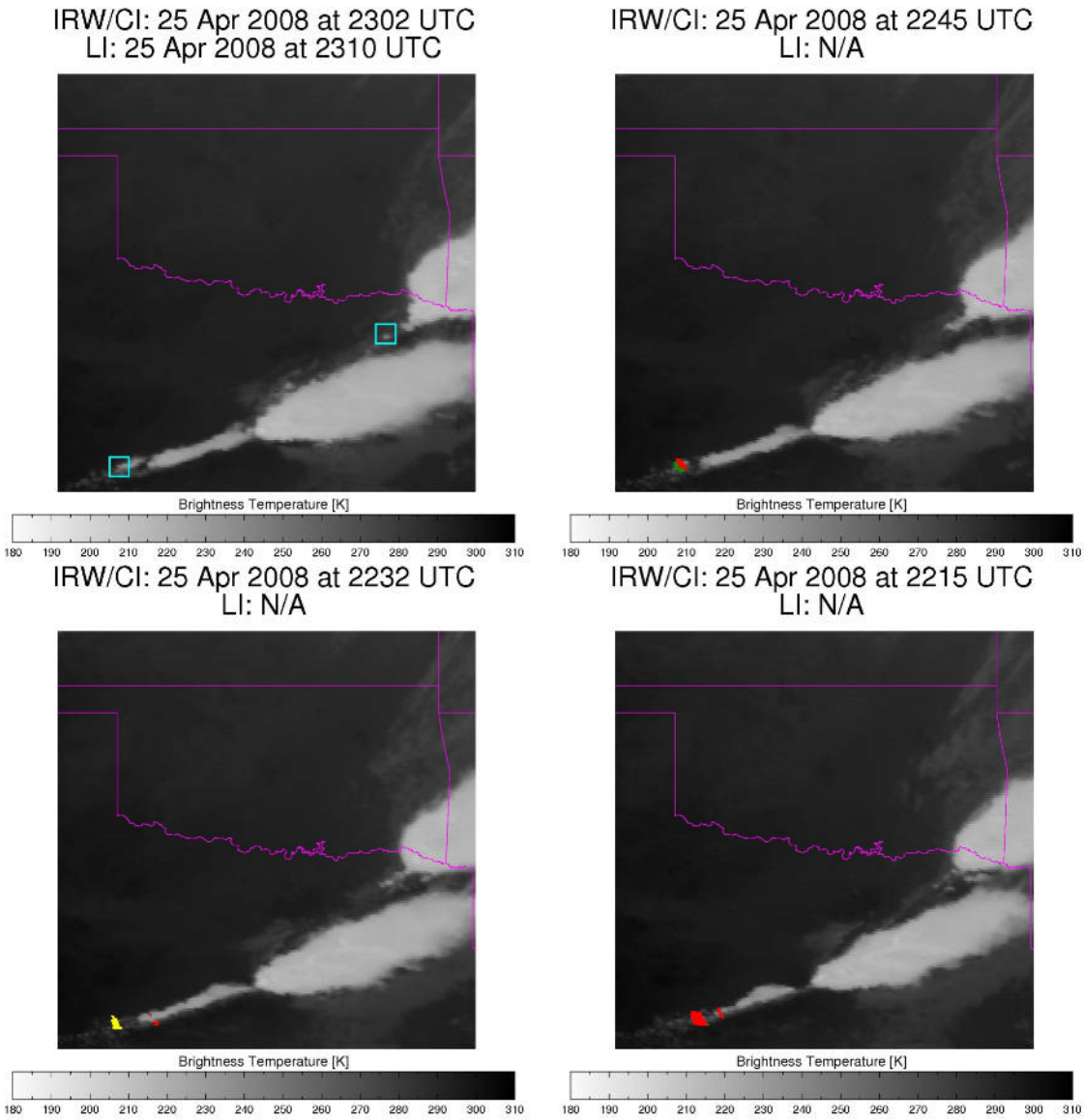

Figure 9. The four-panel image demonstrates how LI events are validated for probability of detection statistics. The underlying imagery is GOES-12 IR-window BT. The green, yellow, and red objects indicate UWCI nowcasts for Pre-CI Cloud Growth, CI Likely, and CI Occurring nowcast categories, respectively. The cyan squares indicate LI locations for the time indicated within the 'LI:' label. The top left panel shows LI valid at 2310 UTC on 25 April 2008 with underlying satellite imagery and UWCI nowcasts at 2302 UTC. The remaining panels show satellite imagery and UWCI nowcasts for previous satellite scans (no LI occurred at these times).

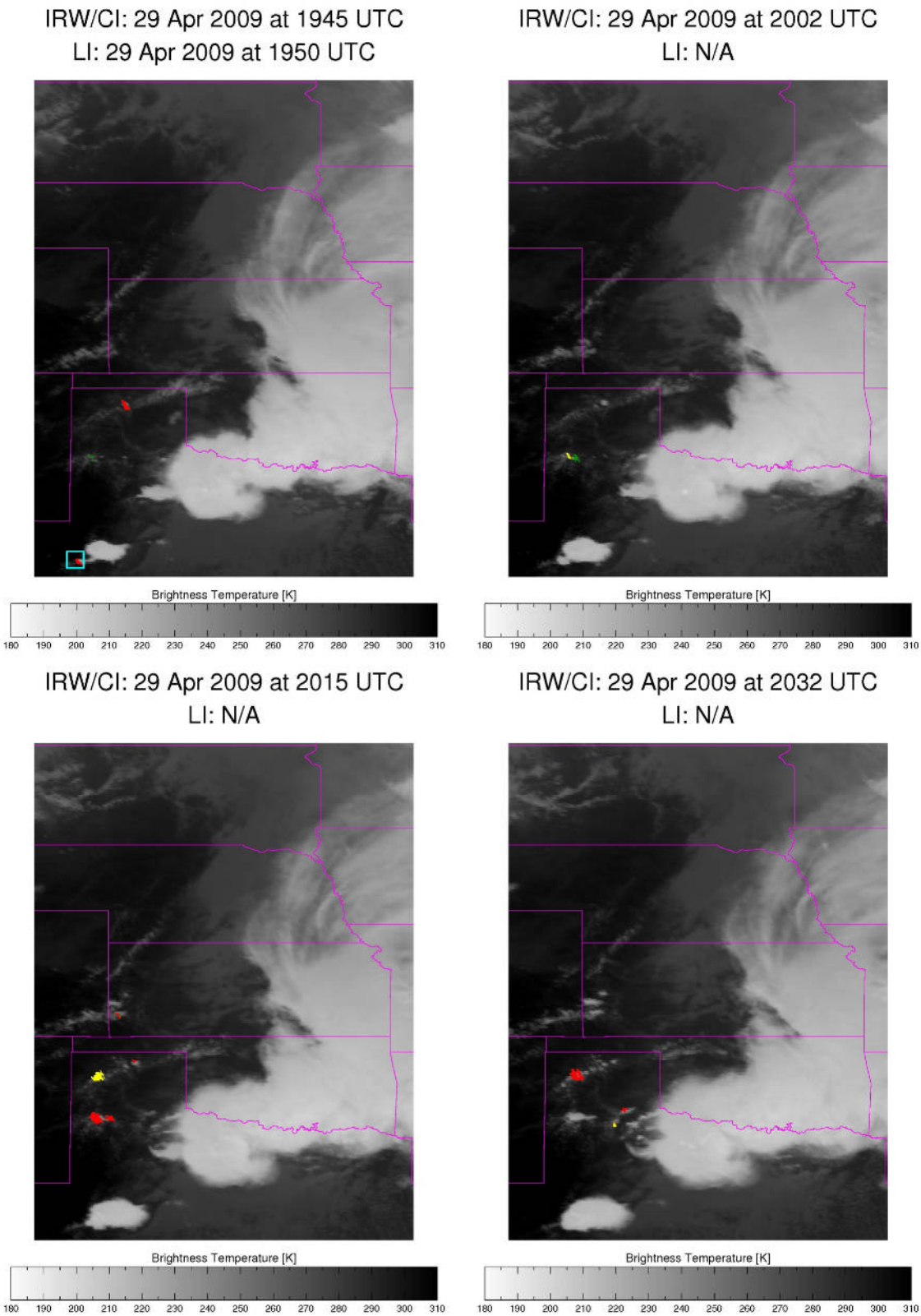

Figure 10. The four-panel image demonstrates how LI events are validated for false alarm ratio statistics. The underlying imagery is GOES-12 IR-Window Brightness Temperature. The green, yellow, and red objects indicate UWCI nowcasts for Pre-CI

Cloud Growth, CI Likely, and CI Occurring nowcast categories, respectively. The cyan squares indicate LI locations for the time indicated within the 'LI:' label. The top left panel shows LI valid at 1950 UTC 29 April 2009 with underlying satellite imagery and UWCI nowcasts at 1945 UTC. The remaining panels show satellite imagery and UWCI nowcasts for subsequent satellite scans (no LI occurred at these times).

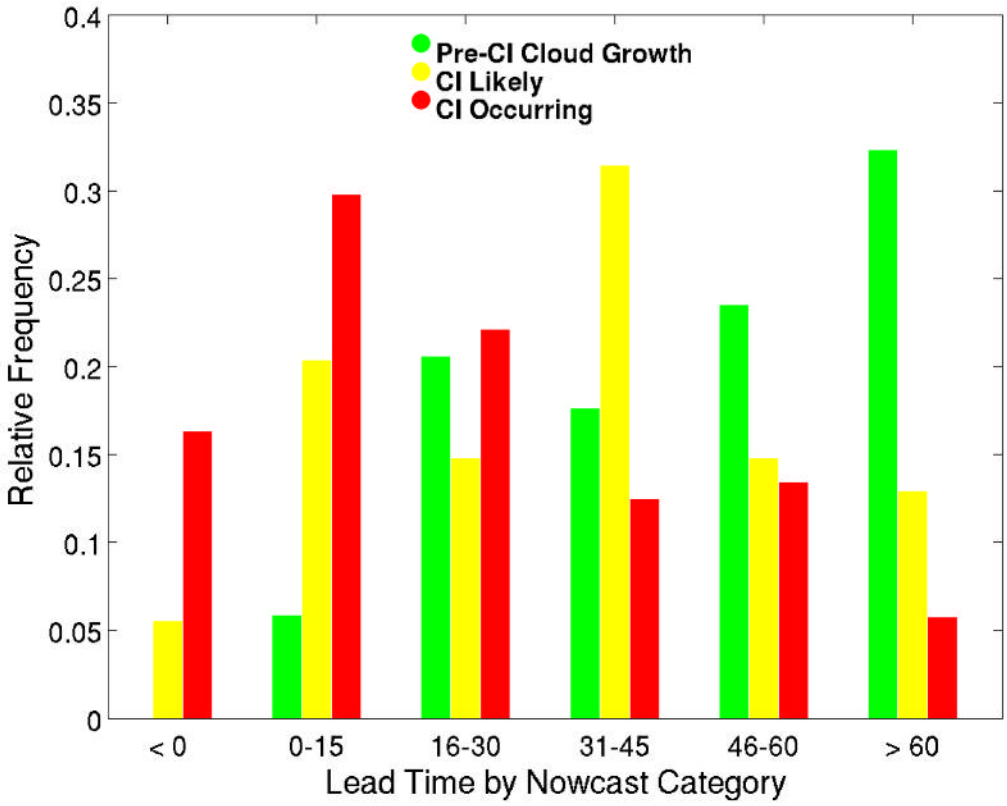

Figure 11. Relative frequency of lead-time by UWCI nowcast category for all successfully nowcast LI events within SPC slight risk or greater regions. Green bars reflect Pre-CI Cloud Growth, yellow bars reflect CI likely category, and red reflect CI occurring category.